

## TURBULENCE DRIVEN BY STELLAR JETS, THE POSSIBILITY AND THE EFFICIENCY

SOMAYEH SHEIKHNEZAMI<sup>1</sup> & MOHSEN ABGHARIAN-AFOUSHTEH<sup>1</sup>,  
*Draft version August 12, 2019*

### ABSTRACT

We investigate the feedback of the stellar jets on the surrounding interstellar gas based on 2D and 3D simulations applying HD and MHD module of PLUTO 4.2 code. The main question we address is whether the stellar jet can be considered as a turbulence driver into the interstellar gas. In addition, we investigate the most effective circumstances in which the driven turbulence is larger and can survive for a longer time scale in the ambient gas. We present a case study of different parameters runs including the jet Mach number, the initial jet velocity field and the background magnetic field geometries and the interacting jets. Also, we study the environmental effects on the jet-gas interaction by considering the non-homogeneous surrounding gas containing the clumps in the model setup. Among different setups, we find that for (1) a higher jet Mach number, (2) a rotating jet, (3) a jet propagating in a magnetized environment, (4) a jet propagating in a non-homogeneous environment, and (5) the interacting jets more fluctuations and random motions are produced in the entrained gas which can survive for a longer time scale. In addition, we perform the 3D simulations of jet-ambient gas interaction and we find that the amount of (subsonic-supersonic) fluctuations increases compared to the axisymmetric run and the entrained gas gains higher velocities in a 3D run. In total, we confirm the previous finding that the stellar jets can transfer the turbulence on neighboring regions and are not sufficient drivers of the large-scale supersonic turbulence in molecular clouds.

*Subject headings:* ISM: jets and outflows - Magnetic fields - Turbulence Methods: Simulation - Magnetohydrodynamics (MHD) - Stars: Pre-main sequence - Formation

### 1. INTRODUCTION

Astrophysical jets are produced by many objects over a wide range of luminosity and spatial scale, from young stellar objects to micro-quasars, and active galactic nuclei (AGN). Jets and outflows carry the mass, energy and angular momentum and have major impacts on the dynamical evolution of their host systems. Jets and outflows besides supernovae, stellar winds, and spiral arms are known as sources providing energy input and turbulence in molecular clouds and star-forming regions (Mac Low & Klessen 2004). Supersonic turbulence is an essential ingredient which can put the constraints on the star formation process. However, the possible dual effects of the turbulence on star formation is controversial. It can compress the material and therefore change the Jeans parameter and provide the condition to form stars. On the other hand, the supersonic turbulence is able to disrupt the clump and decreases the star formation (McKee & Ostriker 2007).

Observational studies show that outflows can transfer sufficient energy to account for cloud turbulent energy (Bally et al. 1996; Knee & Sandell 2000; Bally & Reipurth 2003; Quillen et al. 2005). One of the essential aspects of studying jet feedback on the host systems is the corresponding scale of the system. The jet feedback can be studied on the scale of star-forming clusters or the entire molecular cloud ( $l > 10^4 AU$ ) which is not the concerns of the current paper. In addition, the jet feedback can be constrained to the jet launching area ( $l < 10 AU$ ) including the launching process of jet besides the impact on the host system. There are

numbers of MHD simulations have investigated the jet launching process (Casse & Keppens 2002; Zanni et al. 2007; Casagrande et al. 2010; Sheikhnezami et al. 2012; Stepanovs et al. 2014; Stepanovs & Fendt 2016; Sheikhnezami & Fendt 2015, 2018). However, the jet launching process in combination with the jet feedback needs to be studied deeply. Moreover, the jet feedback can be constrained to the larger scale ( $l < 10^4 AU$ ) in which the impact of jets on the infalling envelopes is considered (Delamarter et al. 2000).

The first study of the stellar outflow feedback was performed by Mac Low (2000). They discuss that the stellar outflow can drive turbulent motions. Later, Banerjee et al. (2007) performed numerical simulations of stellar jets and discuss that the collimated jets from young stellar objects are unlikely drivers of large-scale supersonic turbulence in the molecular cloud. In addition, Cunningham et al. (2009) have carried out simulations of a single outflow interacting with a turbulent medium. They conclude that outflow-driven cavities are able to re-energize turbulent motions in their immediate environment provided that such turbulent motions already exist to disrupt the cavity. There is a vast of literature investigating the driving of the turbulence in their surrounding area at different scales (Carroll et al. 2009; Joung et al. 2009; Wang et al. 2010; Carroll et al. 2010; Hansen et al. 2012; Federrath et al. 2014). However, the efficiency of driving the turbulence by the stellar jet is not completely known.

In the current paper we aim to perform the case study of different stellar jet parameters to investigate the most efficient circumstances of driving the turbulence to the surrounding gas. Here we are mainly interested in high-velocity jets as a potential source of supersonic turbu-

snezami@ipm.ir & m.abghari@outlook.com

<sup>1</sup> School of Astronomy, Institute for Research in Fundamental Sciences (IPM), P.O. Box 1956836613, Tehran, Iran

lence and we do not consider other physical processes like radiation or heating and cooling of the system.

Compared to the previous works, we perform a wider case study both in HD and MHD regimes and we discuss the role of various physical parameters like velocity components or the background magnetite field geometry which have not been studied in details in previous works. We discuss the turbulence generally and we are not constrained just to the supersonic turbulence. The main question we address is whether the stellar jet can deliver the turbulence into the interstellar medium. In addition, we aim to investigate the most appropriate circumstances in which the larger fraction of turbulence can be transferred to the surrounding gas and survive for a longer time scale.

The paper is organized as follows; in section 2 we describe the model setup, initial and boundary conditions. in section 3 we present and discuss the different parameters runs. and in section 4 we summarize the results.

## 2. MODEL SETUP

In this paper, we focus on the interaction of the jet with the interstellar gas to investigate the efficiency of driving the (subsonic-supersonic) turbulence by the stellar jet into the ambient gas. In particular, we study the global effects of the propagation of a formed jet far from the source (star) and thus not constrained by the gravity of the source.

### 2.1. Initial conditions

For our numerical simulations, we use PLUTO code (Astrophysical gas dynamics code, version 4.2, Mignone et al. (2007, 2012)) solving the time-dependent, HD and ideal MHD equations, namely for the conservation of mass, momentum, and energy:

$$\frac{\partial \rho}{\partial t} + \nabla \cdot (\rho \vec{v}) = 0, \quad (1)$$

$$\frac{\partial(\rho \vec{v})}{\partial t} + \nabla \cdot \left( \vec{v} \rho \vec{v} - \frac{\vec{B} \vec{B}}{4\pi} \right) + \nabla \left( P + \frac{B^2}{8\pi} \right) + \rho \nabla \Phi = 0, \quad (2)$$

Here,  $\rho$  is the mass density,  $\vec{v}$  is the velocity,  $P$  is the thermal gas pressure,  $\vec{B}$  stands for the magnetic field, and  $\Phi$  denotes the gravitational potential which is ignored in our model setup since we study the jet area far from the central object.

The total energy density is

$$e = \frac{P}{\gamma - 1} + \frac{\rho v^2}{2} + \frac{B^2}{2} + \rho \Phi. \quad (3)$$

The gas pressure follows a polytropic equation of state  $P = (\gamma - 1)u$  with  $\gamma = 5/3$  and the internal energy density  $u$ . Our model setup includes the jet environment and the surrounding gas in which the jet area has a lower density but is in pressure equilibrium with the ambient gas. The evolution of the magnetic field (for MHD setup) is described by the induction equation (in absence of the diffusive term),

$$\frac{\partial \vec{B}}{\partial t} - \nabla \times (\vec{v} \times \vec{B}) = 0. \quad (4)$$

Including the heating or cooling processes is beyond the goals of the current paper, and we will study the jet propagation in the non-ideal MHD regime, in a future paper.

### 2.2. Numerical setup

Our simulations are performed in axisymmetry applying cylindrical coordinates  $(r, \phi, z)$  and thus the  $z$ -axis is the symmetric axis. We perform the 3D run of jet-gas interaction and present and discuss that run in section 3.5.

The computational domain spans a rectangular grid region applying a uniform spacing in the radial and the vertical direction. The domain extends to  $60 \times 100$  jet radii  $r_{\text{jet}}$  on a grid of  $1200 \times 2000$  cells, resulting in a resolution of  $\Delta r = 0.05$ . For the boundary conditions, the axisymmetry on the rotation axis and the standard PLUTO outflow (zero gradient) condition for the upper  $z$  and outer  $r$  boundary are imposed. On the lower  $z$  boundary, we implement the jet input for the jet area ( $r < 1$ ) and for the rest, the standard PLUTO reflective boundary condition is applied. It should be mentioned that in all runs presented here the injected jet is continuously powered.

For the spatial integration, we use linear reconstruction. In addition, we apply a second-order RK2 scheme for time evolution. We consider TVDLF solver for all runs. For the magnetic field evolution, we apply the constrained transport method ensuring solenodality condition  $\nabla \cdot B = 0$ .

### 2.3. Units and Normalization

We present our results in code units. We choose units in which the density of the ambient gas is unity  $\rho_a = 1$  and if we assume a mean molecular density of  $10^3 \text{ cm}^{-3}$ , a mean molecular mass weight of  $\mu = 2.1$  the gas density of the ambient is  $\rho = 3.51 \times 10^{-21} \text{ gr cm}^{-3}$ . The jet density is lower  $\rho_j = \delta \rho_a$  than the ambient gas where  $\delta$  denotes the the density contrast between the jet and the surrounding gas. In addition, distances are expressed in unit of the jet radius  $r_j$  which is about  $100 \text{ AU}$  in physical expression. The sound speed of the ambient gas is unity  $C_s$  which is about  $1 \text{ kms}^{-1}$  and the unit of the gas velocity corresponds to the sonic Mach number. The physical time unit in our setup is about  $500 \text{ yr}$ .

### 2.4. PROBABILITY DENSITY FUNCTION (PDF)

The turbulence in the literature is known as the random motions of the gas flows at different scales. To investigate the turbulence induced by the stellar jet it is important to use a proper method to estimate the ‘‘induced turbulence’’ in the surrounding gas materials. One of the best way to measure the turbulent motion in a flow is using the probability density function of velocity which has been used by previous authors (see e.g. Banerjee et al. (2007)). To calculate the probability density function, we consider all the volume excited by the jet propagation having the non-zero velocity i.e.,  $v_p = \sqrt{v_r^2 + v_z^2}$ . We consider different velocity bins, i.e.,  $v_i, v_i + dv$  and the probability density function is defined as,

$$P_i(f_i) = w(f_i) / N_{\text{tot}}; \quad (5)$$

**Table 1**

Characteristic parameters of our simulation runs. Here  $\rho_j$  is the jet density,  $v_r$  is the radial velocity of jet,  $v_\phi$  is the jet rotation,  $\rho_a$  is the ambient gas density,  $\delta = \frac{\rho_j}{\rho_a}$  is the ratio of the jet density to the ambient gas density,  $M = \frac{V_j}{c_s}$  is the Mach number which is the ratio of the jet velocity to the sound speed,  $B_r$  is the radial,  $B_z$  is the vertical and  $B_{\text{phi}}$  is the toroidal background magnetic field.

Run	$M$	$V_r$	$V_\phi$	$\delta$	$B_r$	$B_z$	$B_\phi$
<b>HD</b>							
HD1	1	0	0	0.1	-	-	-
HD3	3	0	0	0.1	-	-	-
HD10 (Reference run)	10	0	0	0.1	-	-	-
HD10t	10	0	0	0.1	-	-	-
HD25	25	0	0	0.1	-	-	-
HD3D	10	0	0	0.1	-	-	-
HD10Vr	10	0.01	0	0.1	-	-	-
HD10Vphi	10	0	0.01	0.1	-	-	-
HD-Qcl (quiescent clump)	10	0	0	0.1	-	-	-
HD-Ecl (explosive clump)	10	0	0	0.1	-	-	-
<b>Interacting jets</b>							
HD10-2jet50 (2 jets, second jet at 50)	10	0	0	0.1	-	-	-
HD10-2jet100 (2 jets, second jet at 100)	10	0	0	0.1	-	-	-
HD10-3jet (3 jets)	10	0	0	0.1	-	-	-
<b>MHD</b>							
MHD-Br	10	0	0	0.1	0.001	0	0
MHD-Bz	10	0	0	0.1	0	0.002	0
MHD-Bphi	10	0	0	0.1	0	0	0.001
MHD-Bp	10	0	0	0.1	0.001	0.002	0

1) HD3D is a run in three dimensions.

2) HD10t is a run with the transient jet which is switched off at time 500.

Where  $f_i$  is a function of velocity determining the given velocity in a range of  $(v_i, v_i + dv)$ .  $w$  counts the number of cells that the condition  $f_i$  is valid for them.  $N_{tot}$  is the total number of cells in the computational domain. Thus,  $P_i(f_i)$  is the probability of the condition  $f_i$  in the whole domain. The total probability used to normalize the PDF is,

$$\sum_i P_i = 1. \quad (6)$$

### 3. RESULTS AND DISCUSSIONS

To investigate the efficiency of driving the turbulence by the stellar jets into the ambient gas, We present a case study of different parameters runs including the jet Mach number, the jet velocity field and the background magnetic field geometries and the interacting jets. Also, we discuss the environmental effects on the jet-gas interaction by considering the non-homogeneous surrounding gas containing the clumps in the model setup (see Table 1).<sup>2</sup>

First, we consider the effects of jet Mach number on the jet-gas interaction. As shown in Table 1 we perform runs with different Mach numbers covering the transonic to highly supersonic jet. Figure 4 displays the snapshots of the mass density at late evolutionary stages for runs *HD1*, *HD3*, *HD10*, and *HD25* with Mach numbers of 1, 3, 10 and 25, respectively. An obvious correlation between the jet Mach number and the size of the excited gas is found. In particular, it is observed that the more random motions and more filamentary structures are produced by the jet with the higher Mach number.

<sup>2</sup> To visualize the results we use Python 2.7.13 and Visit 2.13.2 software.

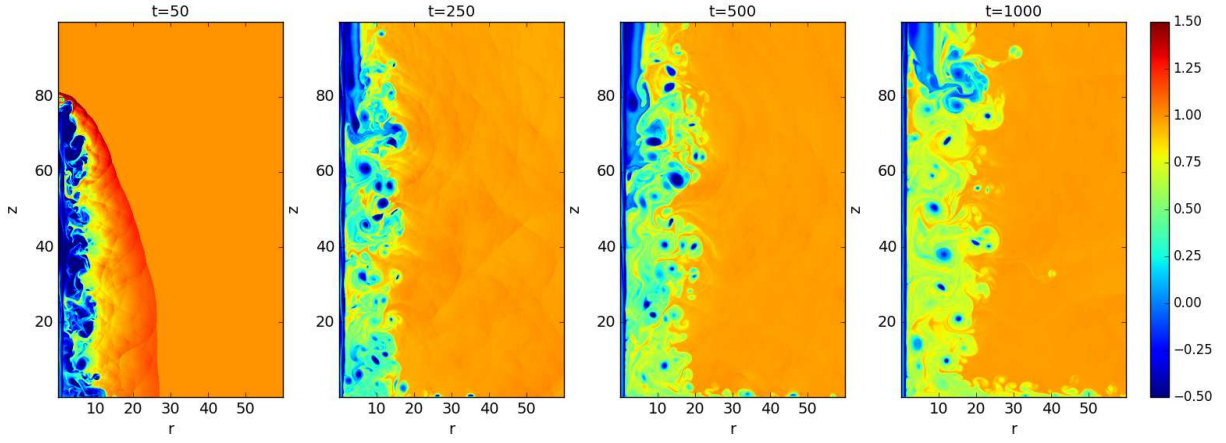
Another useful parameter is the entropy of the gas displaying the energy distribution of the system and is shown in Fig 3. It demonstrates that the jet materials have higher entropy than the entrained gas. As time passes, the excited gas loses the energy, gets slower and reaches a lower entropy level.

We can trace the evolution of the jet and the surrounding gas by considering the probability density function of the velocity, more precisely. To calculate the PDF, we consider the local sound speed  $c = \sqrt{(\gamma p / \rho)}$  of the gas which allows for distinguishing the supersonic and the subsonic features.

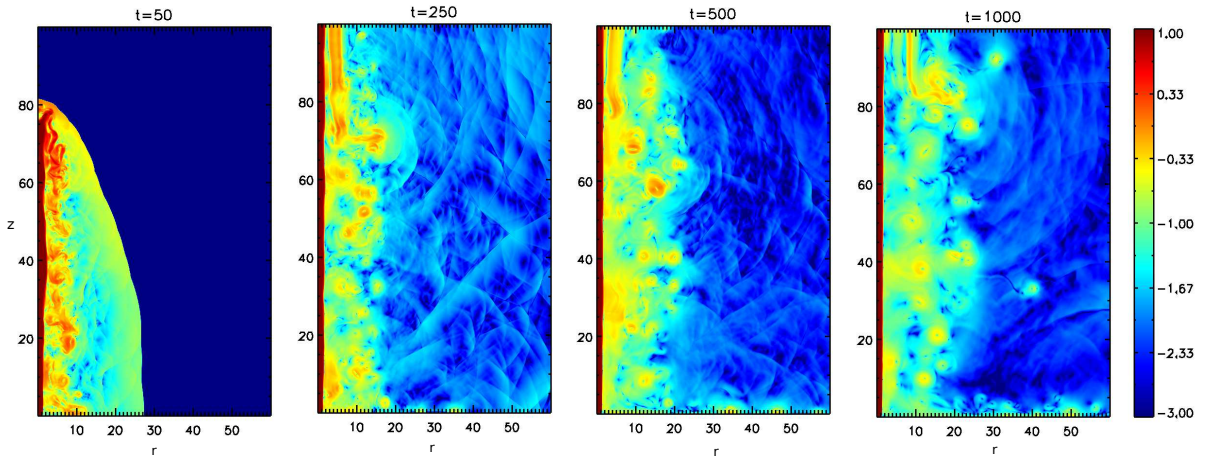
In order to investigate how long the velocity fluctuations produced by the stellar jet can survive in the environment we perform a run including the transient jet called *HD10t* in which the jet engine is switched off after time 500 and considered in the PDF diagram as well.

Figure 6 illustrates the PDF of velocity for reference run, run *HD25* and run *HD10t* with the transient jet at times 50, 500, 1000. It is clearly seen that the transient jet (right panel) does not show any significant supersonic fluctuations after the driving has been stopped. In fact the dying jet displays the decay of the peak of the PDF of velocity after switching off the jet and no super sonic feature is seen after time 500.

Comparing two other runs with Mach number 10 and 25, we find that in both runs, the small fraction of the excited gas is supersonic and the majority of the motions are subsonic. But, the peak of the PDF of velocity stays at higher velocity in run with higher Mach number, which means that the entrained gas has a higher velocity. Also, the velocity map shown in Fig 5 confirms that the entrained gas extends to the larger area and corresponds to the higher velocity in a run with a higher jet Mach number. By passing time, the peak of the PDF of ve-



**Figure 1.** Reference run. Shown are the snapshots of the mass density in Logarithm scale for reference run *HD10* at times 50, 250, 500, 1000.



**Figure 2.** Shown are the snapshots of the poloidal velocity in Logarithm scale,  $v_p = \sqrt{v_r^2 + v_z^2}$ , for reference run *HD10* at times 50, 250, 500, 1000.

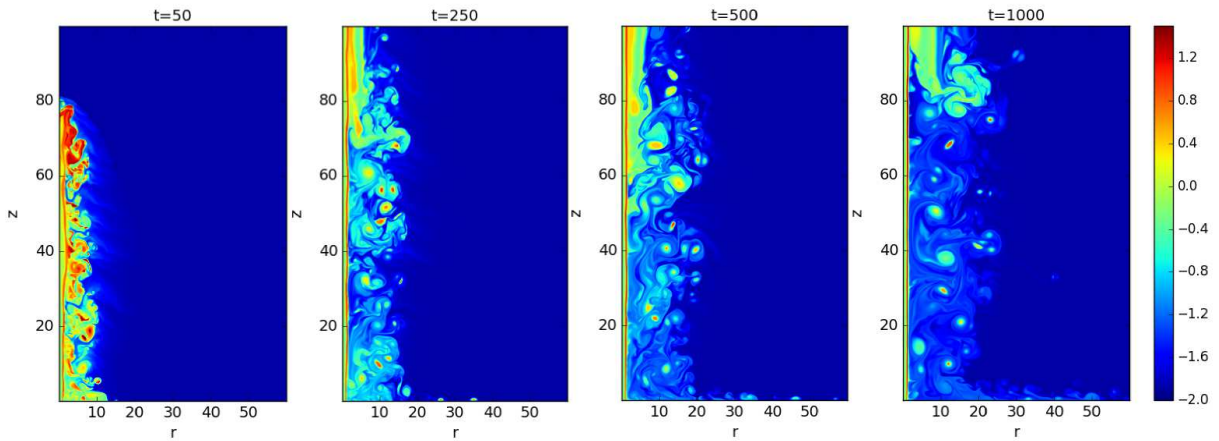


**Figure 3.** Displayed are the snapshots of the entropy of reference run *HD10* at times 50, 250, 500, 1000.

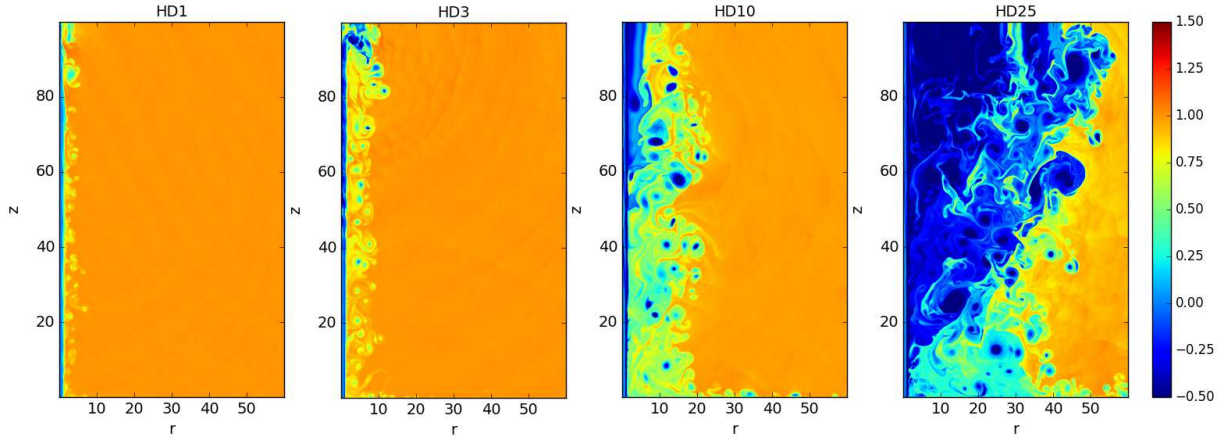


**Figure 4.** Shown are the snapshots of the mass density in Logarithm scale for runs with Mach numbers of 1, 3, 10 and 25 at time 500.

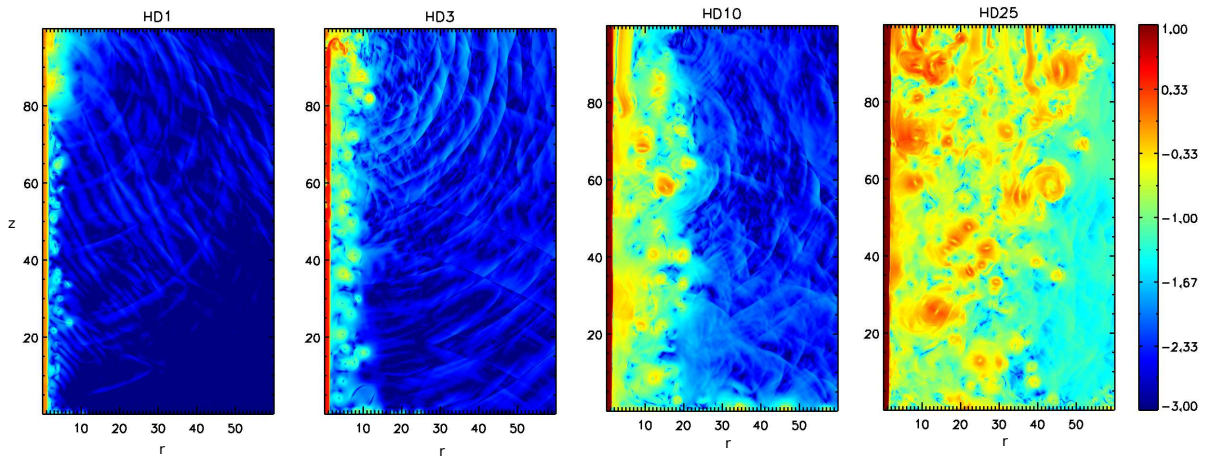


**Figure 5.** Shown are the snapshots of the velocity field in Logarithm scale  $v_p = \sqrt{v_r^2 + v_z^2}$  for runs with Mach numbers of 1, 3, 10 and 25 at time 500

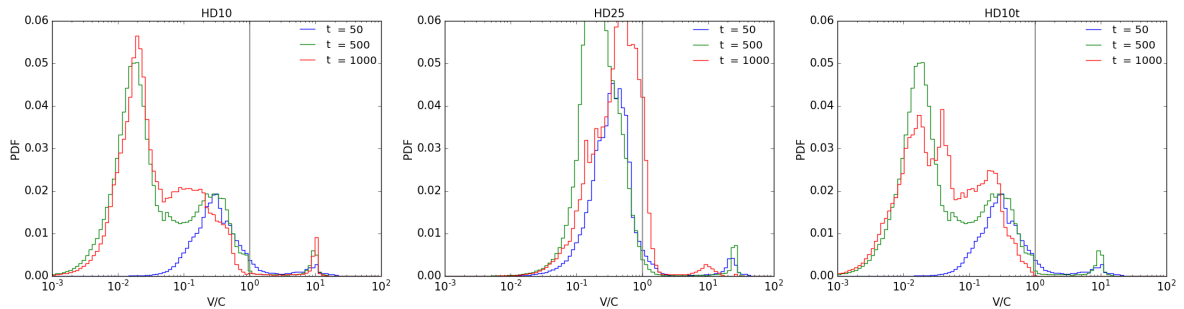


**Figure 6.** Shown are the plots of the probability density function of velocity for run *HD10*, *HD25* and *HD10t* at times 50, 500, 1000. Here  $C$  denotes to the local sound speed of the gas. The vertical line shows the transonic velocity and distinguishes between the subsonic and the supersonic velocities.

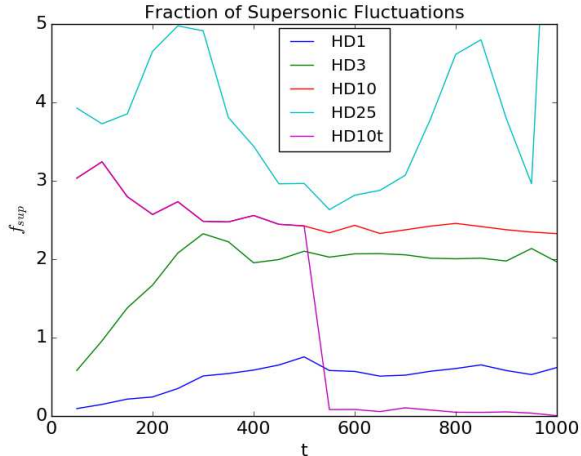


**Figure 7.** Shown is a comparison of the evolution of supersonic features with respect to all gas materials for runs with Mach numbers of 1, 3, 10, 25 and run with the transient jet.

locity moves towards the lower velocities which indicates the decay of the induced turbulence in the entrained gas. In comparison, we do not see a big variation in the position of the peak of the PDF of velocity in run *HD25* with the higher Mach number during the time.

Specifically, it is possible to compare the supersonic part of the gas of all runs and have a better view. Figure 7 illustrates the evolution of the supersonic features with respect to all gas materials for runs applying different Mach numbers and run with the transient jet. It shows that some part of the entrained gas remains supersonic at the late evolutionary stage ( $t=1000$ ). Since the jet with the higher Mach number interacts more strongly and also transfers a larger fraction of energy and angular momentum the size of the excited gas increases and the peak of the PDF of velocity fluctuations stays at larger velocities. It means that the velocity of the injected jet can affect the distribution of the velocity fluctuations and the induced turbulence. Thus, one can conclude that the supersonic turbulence driven by a jet with higher Mach number can survive on a larger time scale. This result is different from Banerjee et al. (2007). They discuss that a slower jet produces a larger fraction of excited gas. It should be noticed that our study corresponds to a different length scale and time scale. Our analysis is constrained to the box size which is about  $10^4$  AUs and is smaller. Also, the time scale in our study is smaller and the surrounding gas is still affected by jet propagation in our simulations. In addition, we discuss the turbulence in general and we are not constrained to the supersonic turbulence which is different from other studies.

### 3.1. Impact of the jet velocity field

Besides the jet Mach number, it is also important to see how different velocity components of the jet materials can influence the jet-ambient gas interaction. To have better comparison and rather wider case study compared to previous works (Banerjee et al. 2007), we perform runs with different initial velocity field of the jet area. Here, we present two runs *HD10Vr* and *HD10Vphi* including the radial and the rotation velocity together with the vertical velocity.

The evolution of their mass density are shown in Fig

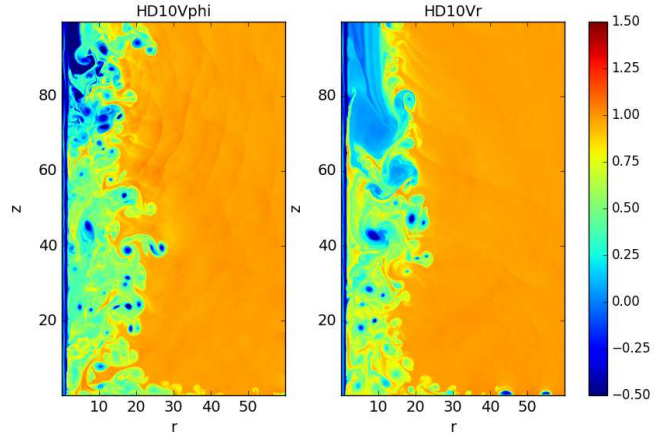


**Figure 8.** Shown are the snapshots of the mass density in Logarithm scale for runs *HD10Vr*, *HD10Vphi* including radial and rotational jet velocity, respectively.

8. Compared to the reference run including the jet radial velocity or the jet rotation increases the size of the entrained gas. This behavior is seen more clearly in the PDF of these two runs (see Fig 9). In comparison, we observe that the runs with additional velocity than  $v_z$  have a wider PDF at the late evolutionary stage. It means that the entrained gas covers a wider range of velocities and the position of the peak of the PDF of velocity stays at the larger velocity. In addition, we find that the peak of the subsonic features in a run applying the rotating jet stays at higher velocities and the stronger effects on the surrounding gas are found. This behavior can be explained by considering the centrifugal force of different runs. Since the rotation is initially chosen to be zero in other runs, the centrifugal force appears only in a run with the rotating jet *HD10Vphi* and the shearing motions between the jet and the ambient gas increase. As we mentioned in the model setup the jet is in pressure equilibrium with the surrounding gas initially. Thus, the jet is stable itself and it interacts by shear instabilities with the surrounding gas. Consequently, we find that the jet rotation enhances the shearing motions which results in turbulent fluctuations in the ambient gas.

### 3.2. Magnetized jet-ambient gas interaction

According to the observational evidence the magnetic field exists in the jet source, inside the jet (Begelman et al. 1984; Crutcher 1999; Ostriker et al. 2001; Marscher et al. 2008; Gómez et al. 2016) and also in the interstellar gas (Crutcher et al. 1999; Brauer et al. 2017; Tahani et al. 2018). It is also believed that jets are most probably magnetically launched and collimated (Blandford & Payne 1982; Pudritz & Norman 1983; Ferreira 1997; Pudritz et al. 2007).

Here, we discuss the effects of the background magnetic field on the jet-ambient gas interaction. We present the MHD simulations applying different background magnetic field geometries, i.e., run *MHD-Br* applying the radial magnetic field, *MHD-Bz* applying the vertical magnetic, run *MHD-Bphi* applying the toroidal magnetic field and run *MHD-Bp* applying the poloidal magnetic field in the domain (see Table 1).

For the sake of comparison, we consider different physical parameters of all MHD runs. First of all, we consider

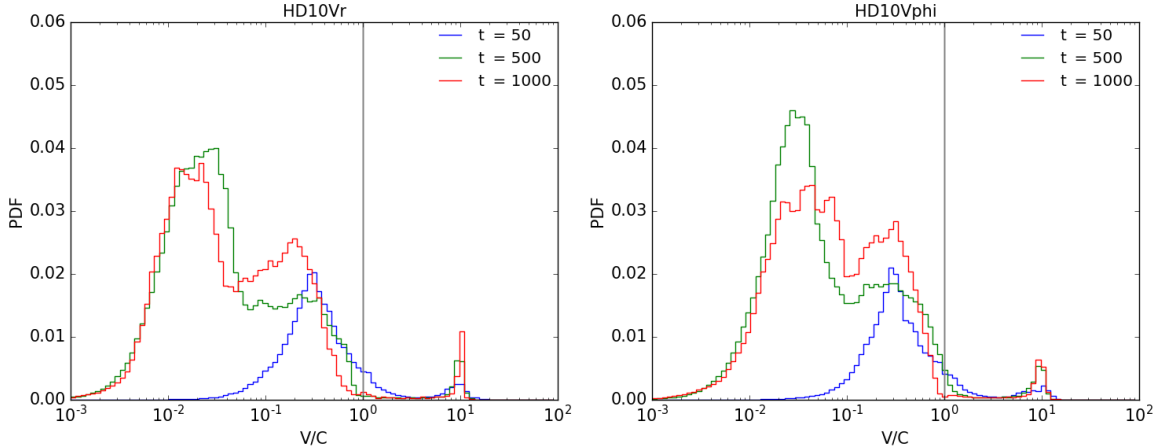


**Figure 9.** Shown are the PDF of velocity for runs *HD10Vr*, *HD10Vphi*, at times  $t = 50$ ,  $t = 500$ ,  $t = 1000$ .

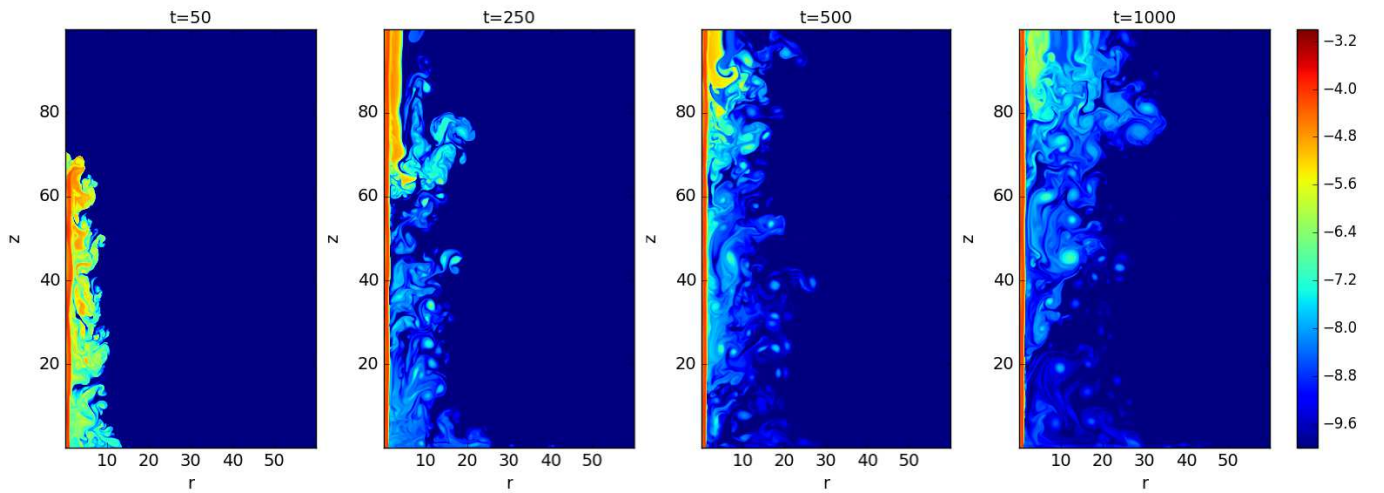


**Figure 10.** Centrifugal force. Shown are the snapshots of the centrifugal force for run *HD10Vphi* including jet rotational velocity.

the mass density distribution of all MHD runs. Figure 11 displays the snapshots of the mass density in Logarithm scale for MHD runs applying different background magnetic fields at time 500. The field lines are shown in black. It is seen that the final structure of the entrained gas depends on the background magnetic field distribution. We observe that a run with the radial or poloidal background magnetic field produces the denser filamentary structures and the entrained gas is confined to a smaller area.

The excited gas materials and the filamentary structure and random motions are seen very nicely in Alfvén Mach number maps. Figure 12 displays the snapshots of the Alfvén Mach number in Logarithm scale for all MHD runs. Here the Alfvén velocity and the Alfvén Mach number are  $v_A = \sqrt{B_p^2/4\pi\rho}$ ,  $M_A = v_p/v_A$ . We observe that the entrained gas is strongly super Alfvénic in all MHD runs that indicates the Alfvén velocity is not large in our MHD setups. It is clearly seen that in run with the poloidal field (last panel) the Alfvén Mach number is lower.

In addition, the entropy maps of all MHD runs shown

in Fig13. We observe that in a run with the toroidal or vertical magnetic field a larger amount of energy is transferred into the ambient gas. It is consistent with the fact that the larger volume of entrained gas is produced and more fluctuations are seen in run with the toroidal or vertical magnetic field. It seems that the magnetic Lorentz force plays an important role and thus we observe different degree of collimation or different accelerations around the jet area.

Considering the PDF of velocity of all MHD runs shown in Fig 14, it is observed that in a run with the radial and poloidal magnetic field the excited gas materials are slower. This behavior is consistent with the mass density pattern which contains the denser features in the entrained gas (see Fig 11). In comparison, the bulk of the subsonic turbulent features in the run with the toroidal field stays at the larger velocities which is consistent with the higher entropy level in this run.

In order to be able to compare the supersonic turbulence, we provide Fig 15 showing the fraction of the domain having supersonic velocities, for all MHD runs. In fact, in all runs a small fraction of supersonic fluctuations is produced in the interstellar gas which is decreasing

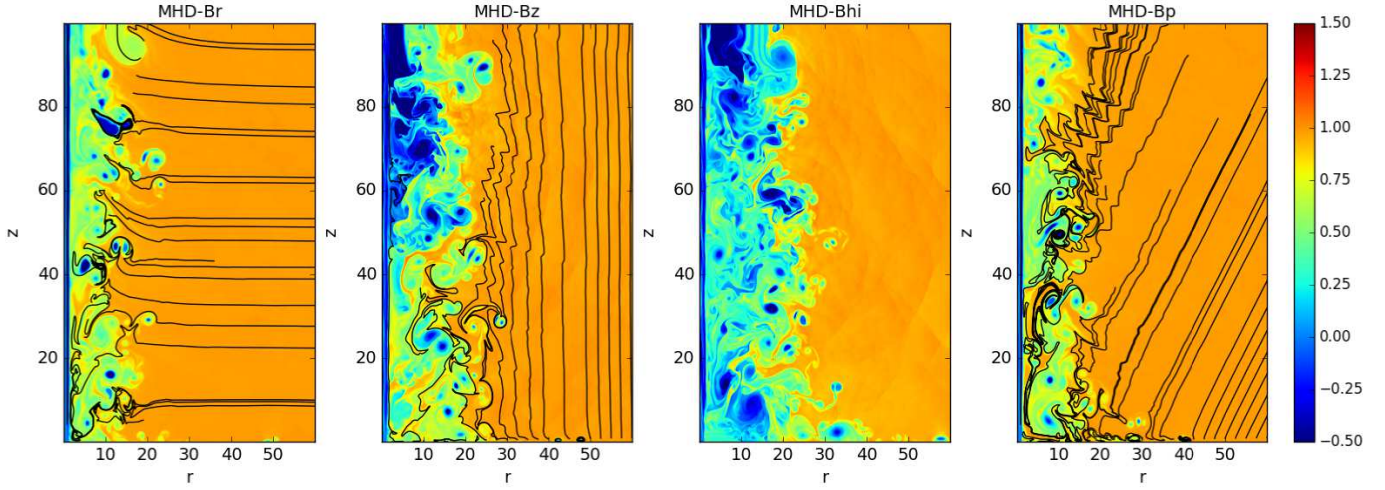


**Figure 11.** Shown are the snapshots of the mass density in Logarithm scale for MHD runs applying different background magnetic fields at time 500. The field lines are shown in black.

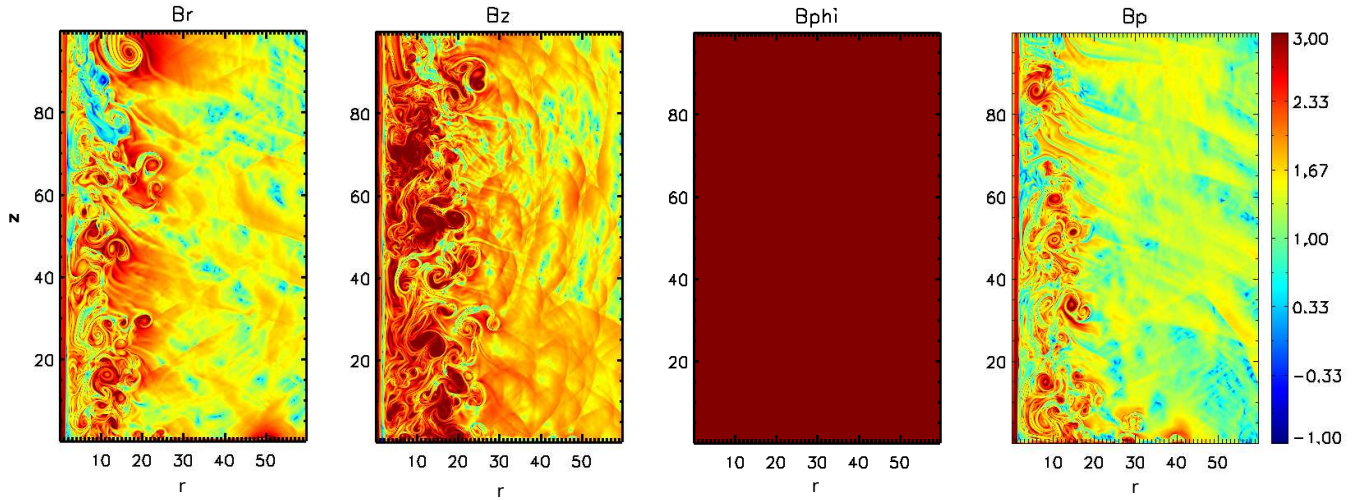


**Figure 12.** Shown are the snapshots of the Alfvén Mach number  $M_A = v_p/v_A$  in Logarithm scale for MHD runs applying different background magnetic fields at time 500.

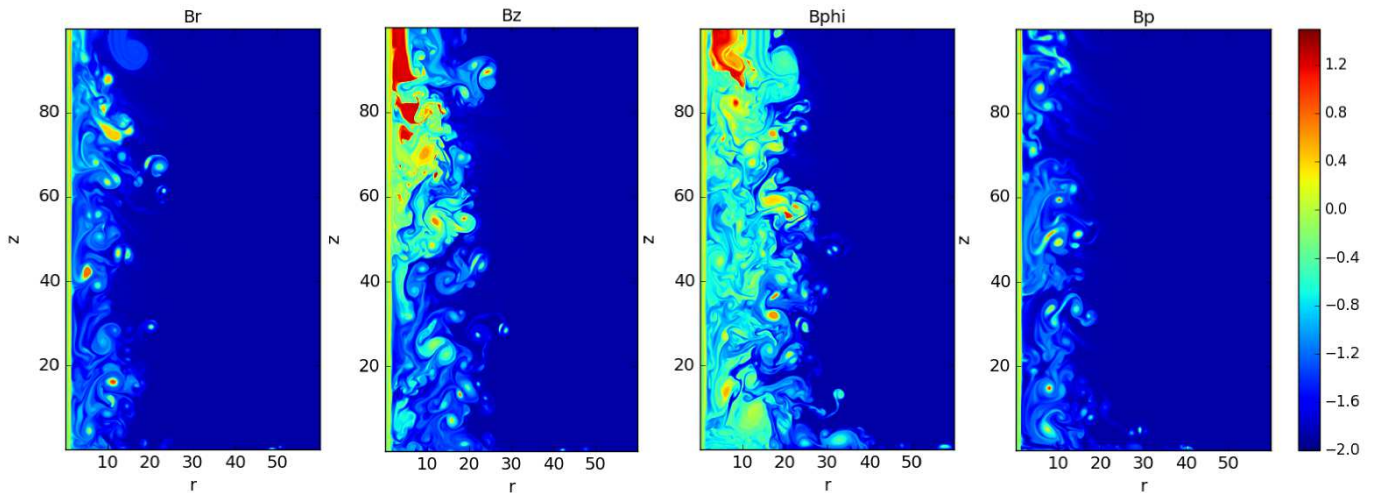


**Figure 13.** Shown are the snapshots of the entropy of gas in Logarithm scale for MHD run applying different background magnetic fields at time 500

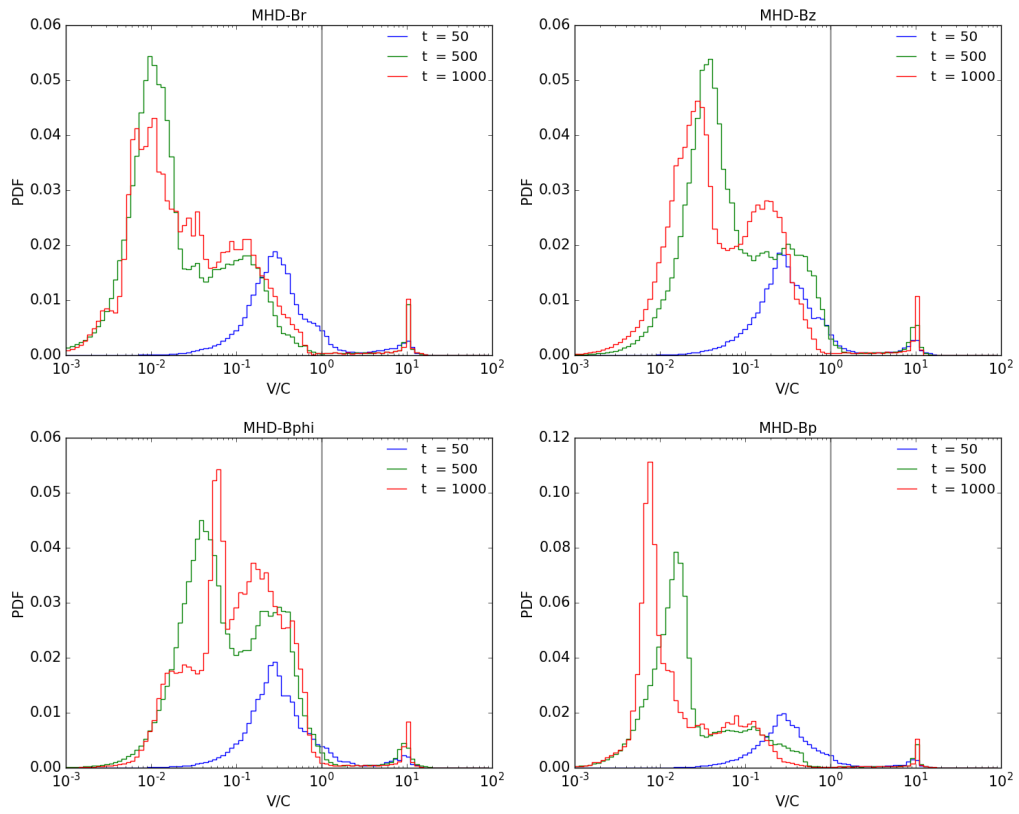


**Figure 14.** Shown are the Probability density functions of velocity for MHD runs at different times.

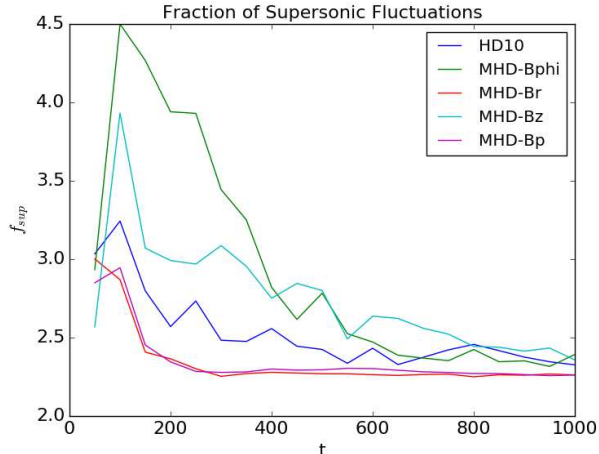


**Figure 15.** Shown is a comparison of the evolution of the supersonic features with respect to all gas materials for the MHD runs and the reference run.

during the time. However, it is seen that in a run with the toroidal field, the fraction of the supersonic features in the ambient gas is higher than reference run and other MHD runs. One physical reason for this behavior is that the run with the radial or the poloidal magnetic field look more collimated and thus the interaction between the jet and the ambient gas is less. Consequently, the shearing motions between the jet and the surrounding gas are less. There should be also other physical reasons which are not known completely and a deeper study is needed.

In total, we find that the run with the toroidal background magnetic field has larger impacts on ambient gas and provides more efficient circumstances to transfer and maintain the turbulence in the surrounding gas. It should be noticed that the entrained gas is almost subsonic and a small fraction of that stays in supersonic regime.

### 3.3. Jet propagation in the clumpy environment

Observational studies demonstrate the interstellar gas is not necessarily homogeneous and jets may encounter clumpy regions during their propagation in the surrounding gas (Krumholz & Tan 2007; Schuller et al. 2009).

In this section, we present the results of simulations in which the jet is propagating into the non-homogeneous interstellar gas and interacts with the clump. We use two different methods to define the clump region.

In the first approach, we define the clump as a region with the higher density but in pressure equilibrium with its neighboring gas, i.e., run *HD-M10cl* and we call it “quiescent clump”. In the second approach, the clump region is defined with a higher density and higher pressure than the neighboring gas, i.e., run *HD-M10pcl* which is called “explosive clump” (see Table 1).

Figure 16 displays the snapshots of the mass density at different times for these two runs. It is observed that the “quiescent clump” exists for a longer time scale and disturbs the jet area locally. Instead the “explosive clump” appears temporary and acts like a violent perturbation and injects energy and disturbs the environment strongly. We recognize that by applying the non homogeneous ambient gas the more entrained gas and random motions are

produced compared to the reference run.

If we compare the PDF of velocity of two clumpy runs we recognize that a considerable fraction of supersonic features are produced, initially in run containing the “explosive clump” (see Fig 17). However, the supersonic fluctuations are not survived until the late evolutionary stage ( $t=1000$ ). It is clearly seen that the peak of the velocity fluctuations moves toward the smaller values reflecting that the turbulence decays rather quickly in this run. It seems that the interaction of the jet and the surrounding gas, in the explosive run is quick and strong but not so efficient to keep the turbulence in the environment for a long time.

As a result, we find that the environmental effects are important in the evolution and maintenance of the turbulent motion in the interstellar gas. In particular, the run containing the long lasting clump “quiescent clump” provides the more efficient circumstances in which the driven turbulence can be maintained for a longer time scale.

### 3.4. Interacting Jets

It is known that the stars are born in cluster environments and thus the stellar outflows might influence the cluster evolution and thus the star formation rate and the mass spectrum within the cluster environments (Li & Nakamura 2006; Wang et al. 2010; Federrath et al. 2014).

However it is still not clear whether the stellar outflows are the main driver of turbulence. To study the efficiency of the stellar outflow as a turbulence driver on a larger scale, we perform some simulations of interacting jets defined in a larger computational domain.

It should be noticed that the more appropriate setup would be a computational domain defined in Cartesian coordinates including two slab jets sufficiently far from each other. However, we perform the simulations of interacting jets in the same cylindrical coordinates to have a better comparison with our reference run.

These simulations are in hydrodynamic regime and shown in Table 1, i.e., run *HD10-2jet50*, *HD10-2jet100* and *HD10-3jet* including two and three interacting jets propagating in the domain.

The snapshots of the mass density of runs including the interacting jets are shown in Fig 18 and 19. It is observed that each jet propagates and produces the shocked area and the entrained materials. By passing time, the interaction between different jets happens. In run *HD10-2jet50*, the interaction happens at earlier time since the separation between jets is smaller.

The interaction between jets leaves a dense region between each two jets and is maintained for a long time. It should be noticed that the jet materials lose energy during the interaction and get slower. During the interaction the jet areas are disturbed and at late evolutionary stage it seem that the jets are suppressed. Thus, not the typical outflows with the large velocity are seen at late evolutionary stages in the environment. Similar behavior is seen in run with three interacting jets (Fig 19). It is seen that two dense regions and the large amount of entrained materials are produced in this run.

Figure 20 illustrates the probability density function of velocity distribution of runs including interacting jets. Regarding the PDF of velocity, we find that the super-

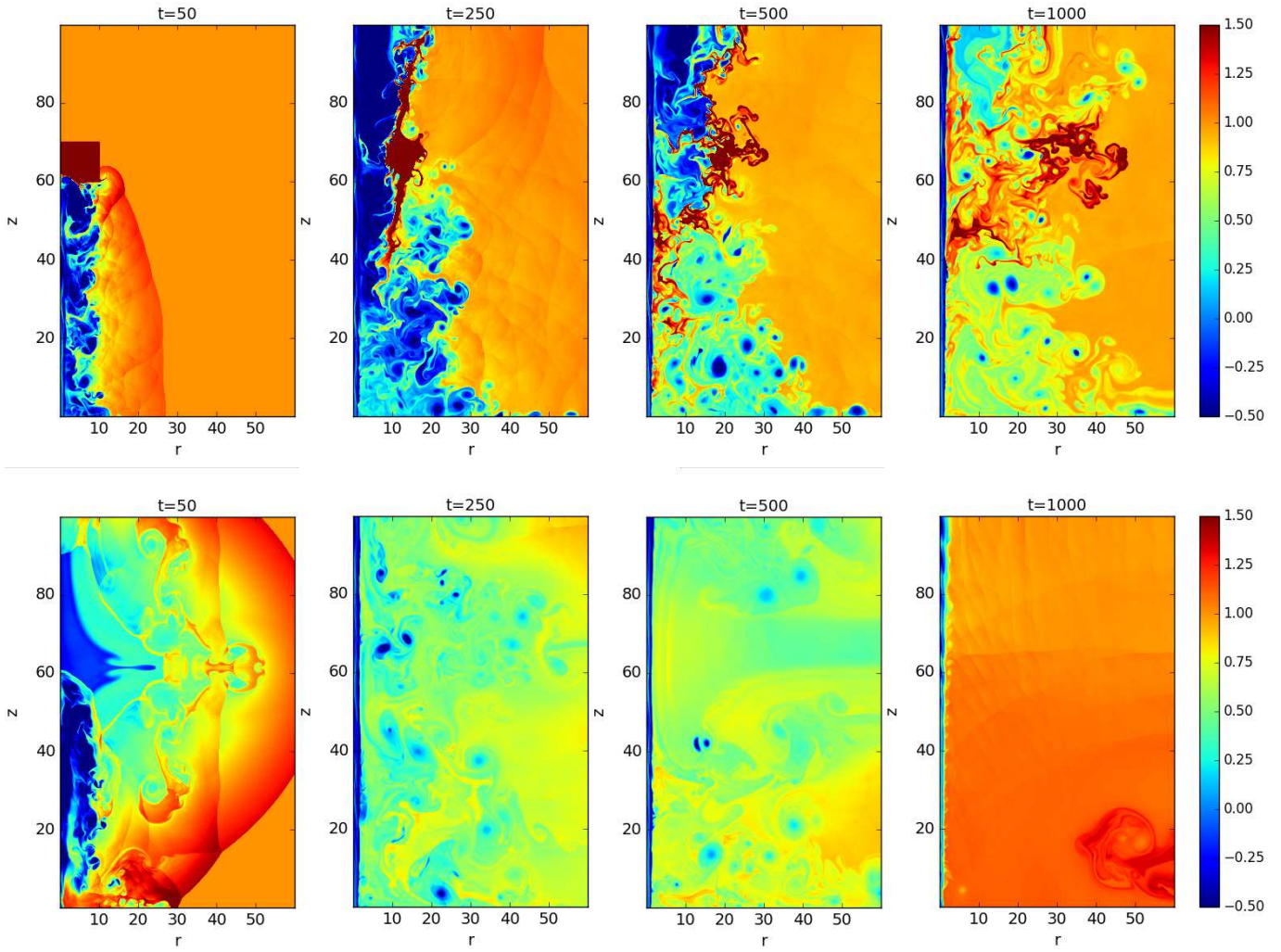


**Figure 16.** Shown are the snapshots of the mass density for run *HD-Qcl* (top) and run *HD-Ecl* at times 50, 250, 500, and 1000 .

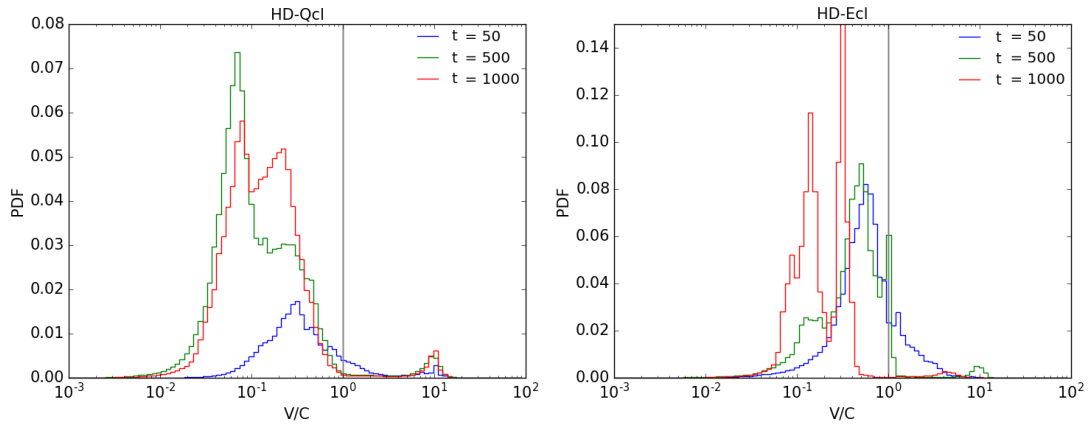


**Figure 17.** Shown are the Probability density functions of velocity for runs, *HD-Qcl* and *HD-Ecl* at different times.

sonic features are not survived for a long time. However, comparing to the reference run the peak of the PDF of velocity is shifted toward the transonic velocities. Specifically, it is seen that the entrained materials have larger velocities in run with interacting jets compared to the reference run with a single jet. The amount of transonic gas in run with three interacting jets enhances.

As a results, we find that including the multiple jets can enhance the amount of fluctuations in the environments which are mainly in subsonic and transonic regime. The supersonic turbulence are suppressed and can not be maintained for a long time scale after the interaction between jets happens.

### 3.5. Jet-ambient gas interaction in 3D

Observations show that the nature does not obey axisymmetry and to have a more natural view of jet-ambient gas interaction we also perform a 3D hydrodynamic simulation, *HD3D* and present the results in this section (see Table 1) .

In particular, we extend the reference model setup to three dimensions and apply similar initial conditions as axisymmetric run. The computational domain is defined in polar coordinates  $(r, \phi, z)$  with the z-axis chosen along the direction of jet rotation axis. The boundary conditions and units are similar to the reference run.

The global evolution of the jet in 3D run is similar to the jet evolution in 2D reference run. The cuts of density mass distribution in three dimensions are shown in Fig 21 at different times. The jet forms the bow shock and excites the ambient gas materials and transfers the energy and turbulence into the surrounding gas. However, some differences are seen in the substructure of the jet-ambient gas which are seen better in the velocity map.

Figure 22 displays the 2D slices of the velocity field in Logarithm scale  $v_p = \sqrt{v_r^2 + v_z^2}$  in  $r$ - $z$  plane for run *HD3D* at different times. It is seen that the excited gas materials extend to the larger radii and have larger velocities compared to the reference run which affects the gas entropy as well. Figure 23 illustrates 2D slices of entropy of the gas in  $r$ - $z$  plane at different times. It is observed that the entrained gas materials have larger entropy compared to the 2D reference run which means that the larger fraction of energy is transferred in 3D run to the ambient gas.

The Probability density function of velocity can give a more accurate picture of the entrained gas evolution. The PDF of velocity for 3D run is shown in Fig 24. We recognize that the amount of (subsonic to supersonic) fluctuations increases compared to the reference run and the excited gas materials gain higher velocities. We observe that the peak of the profile moves toward the larger velocities and the larger fraction of the gas materials stays in supersonic regime even at late evolutionary stage.

To investigate the accurate reasons of the differences seen in 3D run compared to axisymmetric run the detailed studies are required which would be the aim of another paper. However, we should consider some reasons which may play role.

It is known from the computational fluid dynamics that to solve the Navier-Stokes equations, the act of discretizing the equations necessarily replaces terms in the equa-

tions with approximations. These approximations can be represented as an additional diffusive term, which is referred to in the literature as numerical diffusion, or numerical viscosity. We should notice that in 3D run, we apply a lower resolution (to save computing time) which makes the equilibrium more unstable. In particular, the lower resolution implying a somewhat higher numerical diffusivity (viscosity) that results in the numerical heating and thus increases the entropy of the gas materials. Consequently, the amount of the fluctuations in the surrounding gas increases.

Another reason may refer to the stability of the jet-ambient gas system in three dimensions. There are some literature have studied the jet stability applying 3D hydrodynamic simulations (Hughes et al. 2002) or 3D MHD simulations (Xu et al. 2000; Porth 2013; Keppens et al. 2013; Mignone et al. 2013). It is known from instability studies, that some of the instabilities develop differently in three dimensions (like Magneto-rotational instability (Rembiasz et al. 2016)). In addition, some substructures and non-axisymmetric effects are observable just in 3D simulations. In our model setup, since the jet is in pressure equilibrium with the surrounding gas the jet interacts by shear motions with the surrounding gas. By doing the 3D simulation of jet-ambient gas the shear motions in azimuthal direction strengthen which influence the stability of the system. In fact, the shear instability is not really considered in the axisymmetric run.

In total, we find that by using the full 3D simulation the larger fraction of the fluctuations are produced in the surrounding gas compared to the axisymmetric run and the entrained gas gains higher velocities in a 3D run. In particular, it is seen that the larger fraction of the gas materials stays in supersonic regime even at late evolutionary stage in the 3D run.

## 4. CONCLUSION

In this work, we have presented a detailed study of feedback from protostellar jets based on simulations of a polytropic supersonic jet interacting with the denser but in pressure equilibrium with the interstellar gas. The presented simulations are performed in 2D and 3D applying the HD and MHD module of PLUTO 4.2 code. The main question we address is whether the stellar jets can deliver the turbulence into the surrounding gas. In addition, we investigate the most effective circumstances in which the driven turbulence is larger and can survive for a long time scale.

We peresented a case study of different parameters runs including the jet Mach number, the initial jet velocity field and the background magnetic field geometries and the interacting jets. In addition, we studeid the environmental effects on the jet-gas interaction by considering the non-homogeneous surrounding gas containing the clumps in the model setup.

We used a statistical measurement of velocity, namely, the velocity probability density function (PDF), to quantify whether the main contributions of the excited motions, stays in subsonic or supersonic regime.

We have obtained the following results.

- (1) We performed runs with different jet Mach numbers covering the range of transonic to highly supersonic

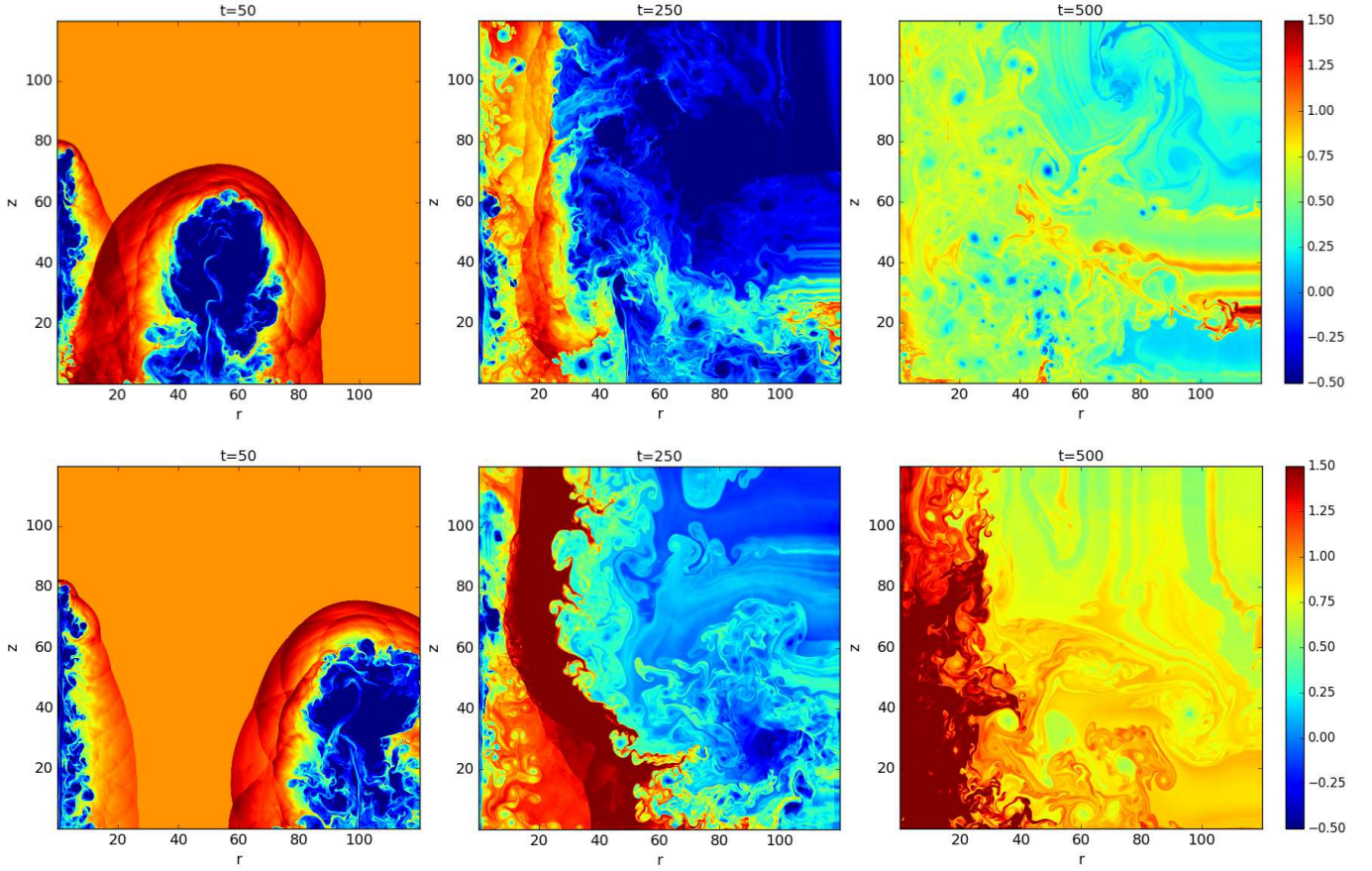


**Figure 18.** Interacting jets. Shown are the snapshots of the density mass of runs including the interacting jets, i.e., run *HD10-2jet50* with (top) and *HD10-2jet100* (middle) with the position of the second jet at 50 and 100 at times 50, 250, 500.

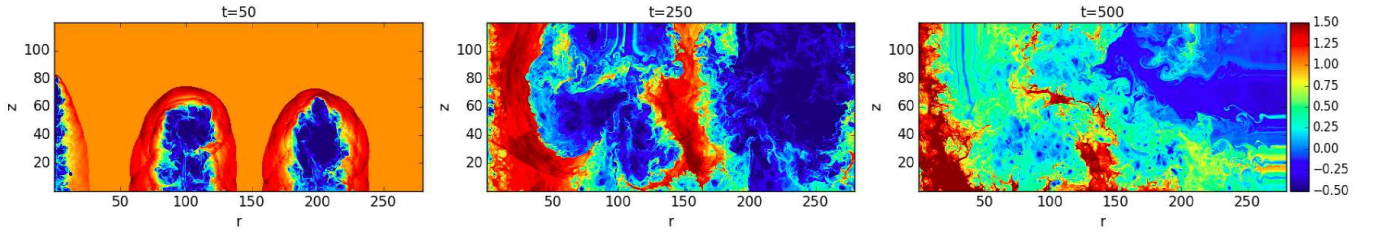


**Figure 19.** Shown are the snapshots of the density mass of run *HD10-3jet* including three interacting jets at times 50, 250, 500.

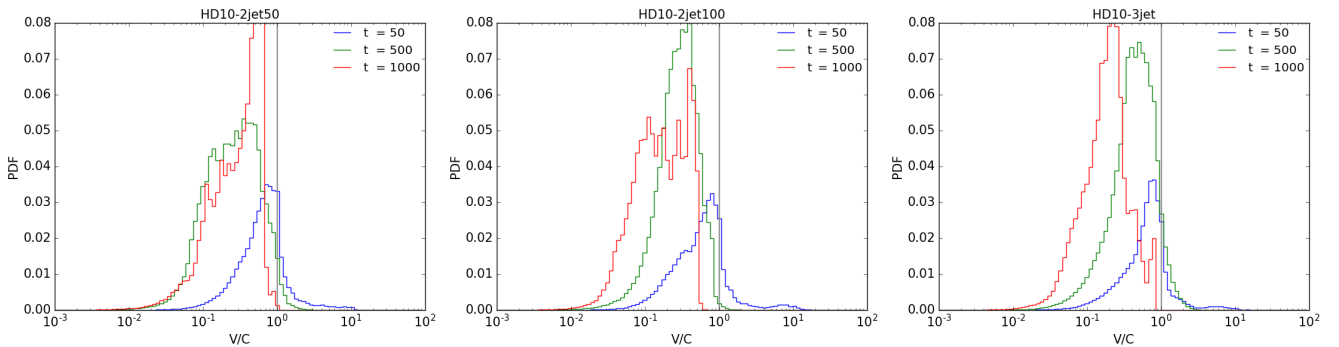


**Figure 20.** Shown are the plots of the probability Density Function of velocity for run *HD10-2jet50*, *HD10-2jet100* and *HD10-3jet* including interacting jets at times 50, 500, 1000.

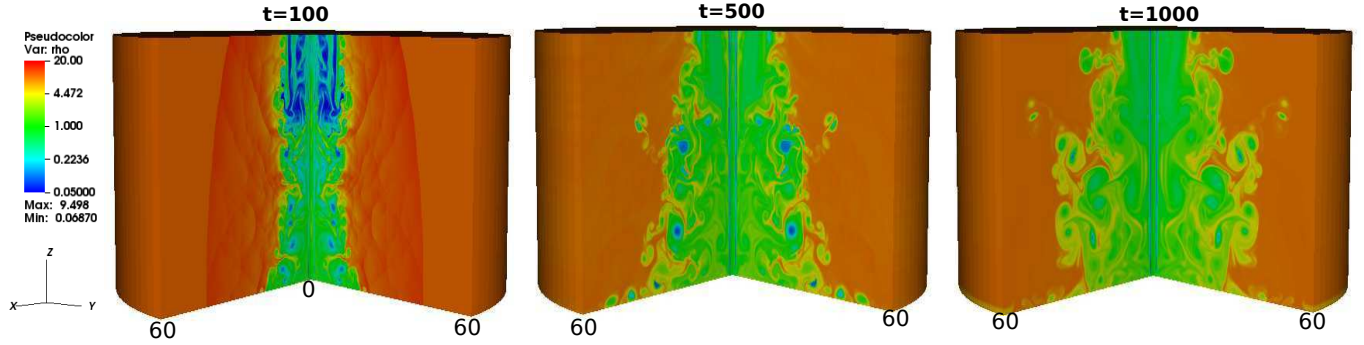


**Figure 21.** 3D evolution of jet-ambient gas system. Shown are the cuts of the mass density distribution in three dimensions for run *HD3D* at times  $t = 100, 500, 1000$ .

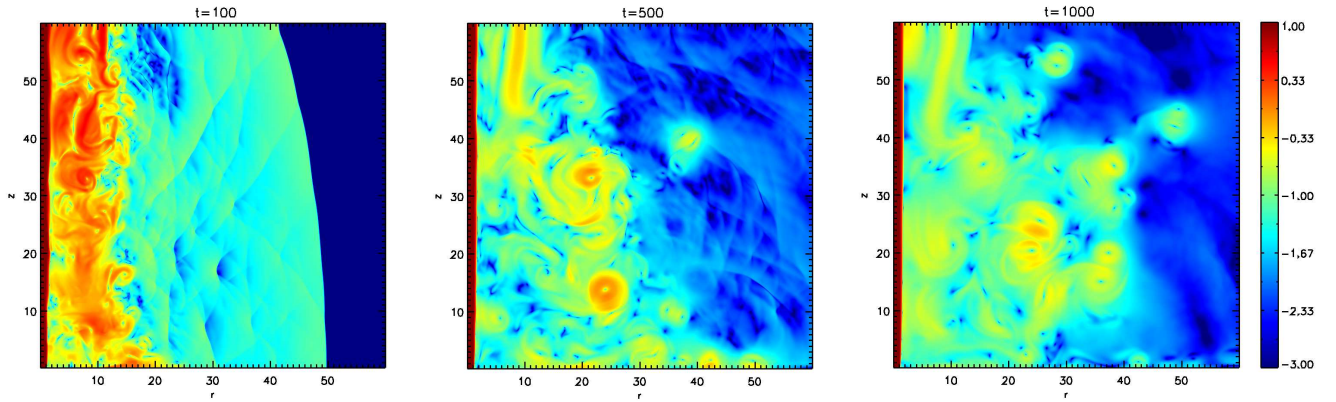


**Figure 22.** Shown are 2D slices of the velocity field in Logarithm scale  $v_p = \sqrt{v_r^2 + v_z^2}$  in  $r-z$  plane for run *HD3D* at times  $t = 100, 500, 1000$ .

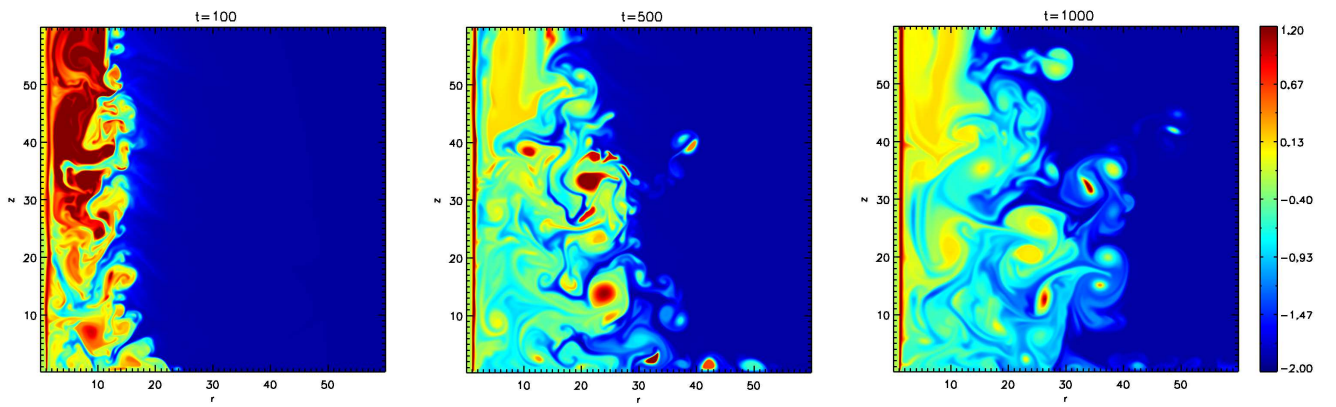


**Figure 23.** Shown are 2D slices of the entropy in Logarithm scale in  $r-z$  plane for run *HD3D* at times  $t = 100, 500, 1000$ .

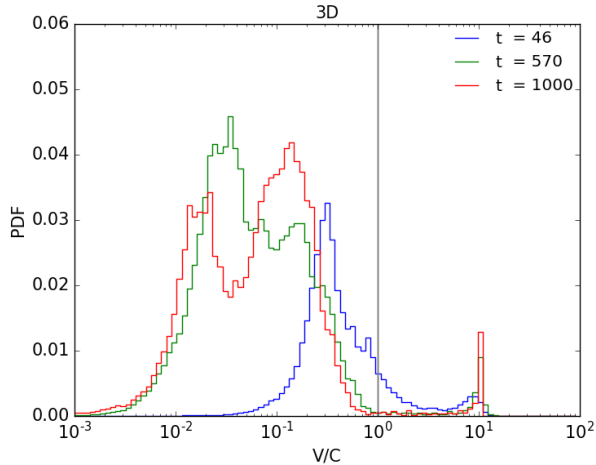


**Figure 24.** Shown are the plots of the probability Density Function of velocity for run *HD3D* at times 50, 500, 1000.

stellar jets. We found a clear correlation between the excited gas and the jet Mach number. By increasing the jet Mach number a faster continues jet is injected into the outer environment and the stronger interaction with ambient gas happens. We recognized that a more powerful jet is a better candidate to drive and maintain the turbulence in the surrounding gas. This result is different from some previous works since we study the jet-ambient gas at different time scale and for a different length scale.

(2) In addition, we performed runs with different jet velocity distributions to investigate which velocity components has a larger impact on the jet-ambient gas interaction. We found that the jet rotation produces the larger shearing motion which results in a more excited gas in the interstellar gas. As we mentioned in the model setup the jet is in pressure equilibrium with the surrounding gas initially. Thus, the jet is stable itself and mostly interact by shear instabilities with the surrounding gas. Including the jet rotation increases the shearing motion between the jet and the ambient gas and produces more velocity fluctuations or turbulence in the entrained gas.

(3) Moreover, we investigated the effects of the background magnetic field on the turbulence driven by stellar jets. Especially, we found that in run with the toroidal background magnetic field, the larger interaction of jet material and the ambient gas happens and the more energy input is produced which is most probably due to the larger shearing motion between the jet and the ambient gas.

(4) Also, we studied the environmental effects on driving process of turbulence by stellar jets. We performed simulations of jet interacting with the non-homogeneous environment containing the clump. We defined two different clumps, one with the higher density but in pressure equilibrium with its neighboring gas called “quiescent clump” and the one called “explosive clump” with over density and over pressure with respect to the neighboring materials. In general, we found that the environmental effects are important in the evolution and

maintenance of the turbulent motion in the interstellar gas. In particular, the run containing the long lasting clump “quiescent clump” provides the circumstances in which the driven turbulence can be maintained for a longer time scale.

(5) To study the efficiency of the stellar outflow as a turbulence driver on a larger scale (like cluster environment), we performed simulations of interacting jets propagating in a larger computational domain. We found that the amount of subsonic and transonic fluctuations enhances but the supersonic turbulence is suppressed and can not be maintained for a long time scale after interaction between jets happens.

(6) In order to have a more realistic setup of jet-ambient gas interaction we extended our model setup to three dimensions and performed a 3D simulation in HD regime. We found that the 3D run displays the similar global evolution of jet to our 2D reference run but some differences are seen in the substructure of the jet-ambient gas. We found that the amount of (subsonic to supersonic) fluctuations increases and the excited gas materials gain higher velocities in the 3D run. Also, we recognized that the larger fraction of the gas materials stays in supersonic regime even at late evolutionary stage compared to the axisymmetric run.

Consequently, we confirm the previous studies on turbulence driven by protostellar jets that they induce the turbulence on neighboring region and are not the proper drivers of large-scale supersonic turbulence in molecular clouds. Although, they are considerable candidate in driving turbulent motions into the surrounding gas and in a smaller scale.

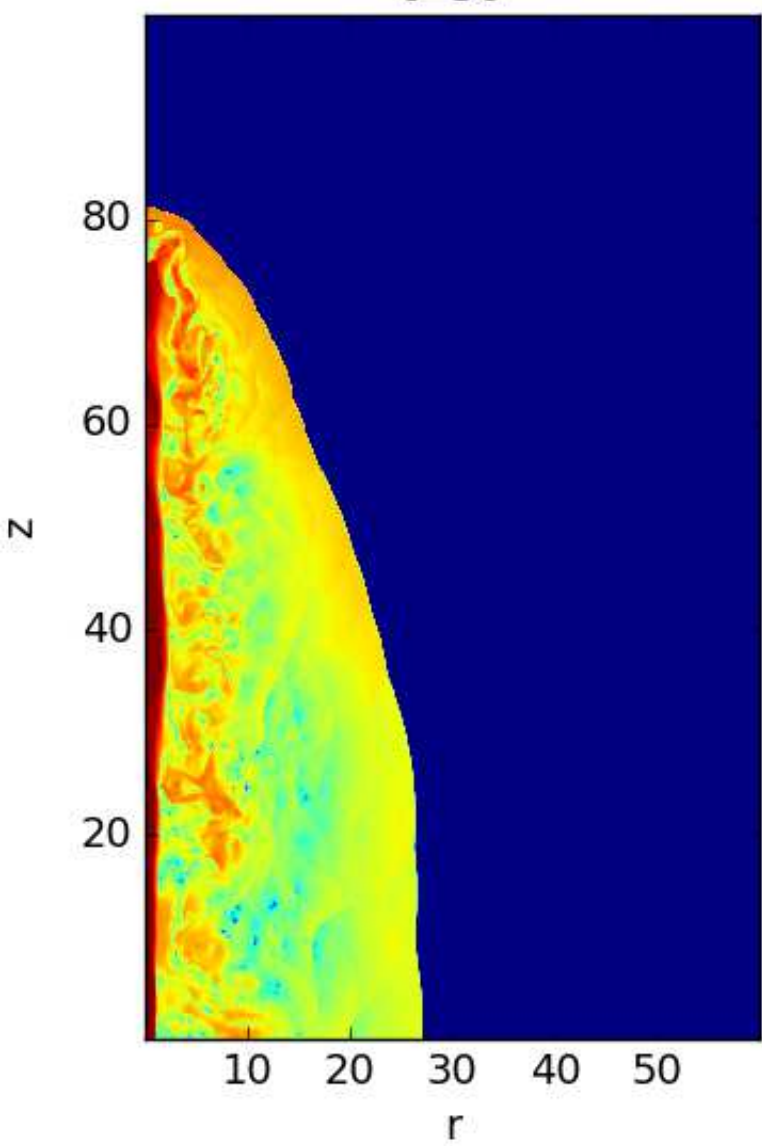
We thank Andrea Mignone and the PLUTO team for the possibility to use their code. We thank Christian Fendt for valuable comments. Our simulations were performed on the IPM cluster of the institute for research in fundamental sciences and Isaac Cluster of Max Planck institute for Astronomy (MPIA). This work was financed by the institute for research in fundamental sciences (IPM). We thank an unknown referee for suggestions that improved the presentation of the paper.

## REFERENCES

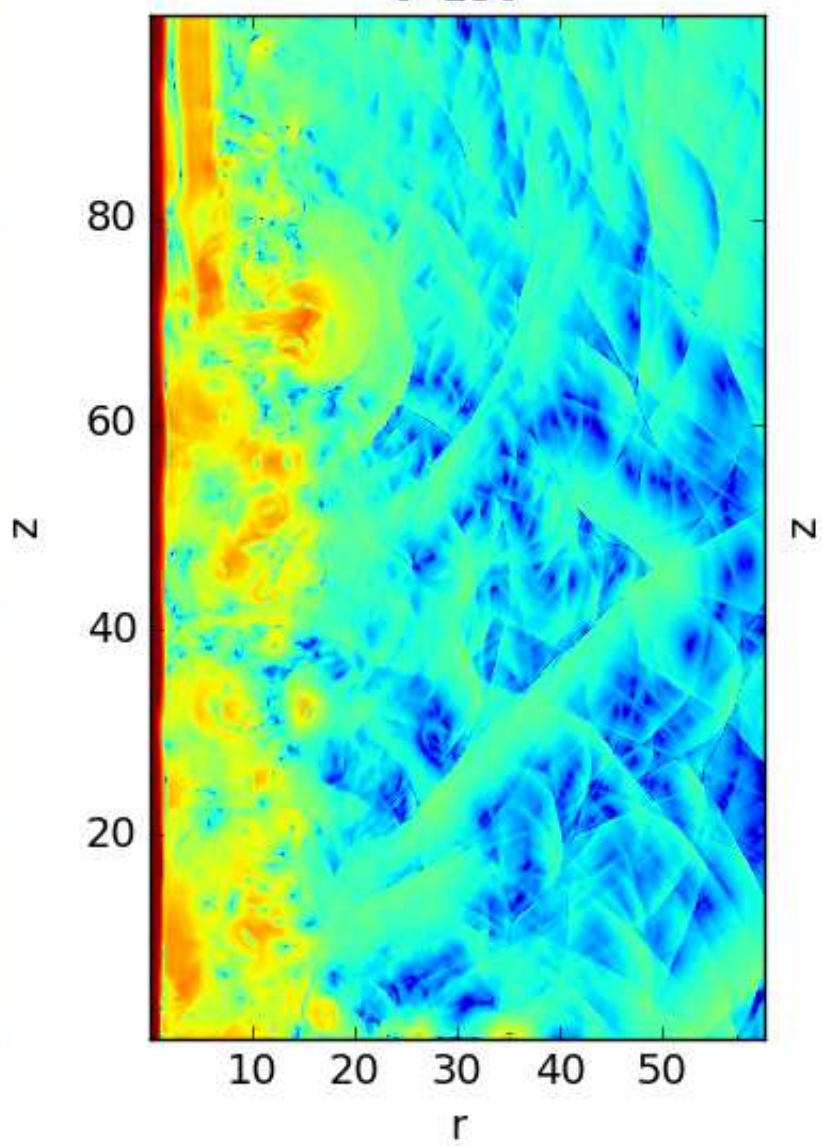
- Bally, J., Devine, D., & Alten, V. 1996, *ApJ*, 473, 921  
 Bally, J. & Reipurth, B. 2003, *AJ*, 126, 893  
 Banerjee, R., Klessen, R. S., & Fendt, C. 2007, *ApJ*, 668, 1028  
 Begelman, M. C., Blandford, R. D., & Rees, M. J. 1984, *Reviews of Modern Physics*, 56, 255  
 Blandford, R. D. & Payne, D. G. 1982, *MNRAS*, 199, 883  
 Brauer, R., Wolf, S., Reissl, S., & Ober, F. 2017, *A&A*, 601, A90  
 Carroll, J. J., Frank, A., & Blackman, E. G. 2010, *ApJ*, 722, 145  
 Carroll, J. J., Frank, A., Blackman, E. G., Cunningham, A. J., & Quillen, A. C. 2009, *ApJ*, 695, 1376  
 Casagrande, L., Ramírez, I., Meléndez, J., Bessell, M., & Asplund, M. 2010, *A&A*, 512, A54  
 Casse, F. & Keppens, R. 2002, *ApJ*, 581, 988  
 Crutcher, R. M. 1999, *ApJ*, 520, 706  
 Crutcher, R. M., Troland, T. H., Lazareff, B., Paubert, G., & Kazès, I. 1999, *ApJ*, 514, L121  
 Cunningham, A. J., Frank, A., Carroll, J., Blackman, E. G., & Quillen, A. C. 2009, *ApJ*, 692, 816  
 Delamarter, G., Frank, A., & Hartmann, L. 2000, *ApJ*, 530, 923

- Federrath, C., Schrön, M., Banerjee, R., & Klessen, R. S. 2014, *ApJ*, 790, 128
- Ferreira, J. 1997, *A&A*, 319, 340
- Gómez, J. L., Lobanov, A. P., Bruni, G., Kovalev, Y. Y., Marscher, A. P., Jorstad, S. G., Mizuno, Y., Bach, U., Sokolovsky, K. V., Anderson, J. M., Galindo, P., Kardashev, N. S., & Lisakov, M. M. 2016, *ApJ*, 817, 96
- Hansen, C. E., Klein, R. I., McKee, C. F., & Fisher, R. T. 2012, *ApJ*, 747, 22
- Hughes, P. A., Miller, M. A., & Duncan, G. C. 2002, *ApJ*, 572, 713
- Joung, M. R., Mac Low, M.-M., & Bryan, G. L. 2009, *ApJ*, 704, 137
- Keppens, R., Porth, O., Monceau-Baroux, R., & Walg, S. 2013, *Plasma Physics and Controlled Fusion*, 55, 124038
- Knee, L. B. G. & Sandell, G. 2000, *A&A*, 361, 671
- Krumholz, M. R. & Tan, J. C. 2007, *ApJ*, 654, 304
- Li, Z.-Y. & Nakamura, F. 2006, *ApJ*, 640, L187
- Mac Low, M.-M. 2000, in *ESA Special Publication*, Vol. 445, *Star Formation from the Small to the Large Scale*, ed. F. Favata, A. Kaas, & A. Wilson, 457
- Mac Low, M.-M. & Klessen, R. S. 2004, *Reviews of Modern Physics*, 76, 125
- Marscher, A. P., Jorstad, S. G., D’Arcangelo, F. D., Smith, P. S., Williams, G. G., Larionov, V. M., Oh, H., Olmstead, A. R., Aller, M. F., Aller, H. D., McHardy, I. M., Lähteenmäki, A., Tornikoski, M., Valtaoja, E., Hagen-Thorn, V. A., Kopatskaya, E. N., Gear, W. K., Tosti, G., Kurtanidze, O., Nikolashvili, M., Sigua, L., Miller, H. R., & Ryle, W. T. 2008, *Nature*, 452, 966
- McKee, C. F. & Ostriker, E. C. 2007, *ARA&A*, 45, 565
- Mignone, A., Bodo, G., Massaglia, S., Matsakos, T., Tesileanu, O., Zanni, C., & Ferrari, A. 2007, *ApJS*, 170, 228
- Mignone, A., Striani, E., Tavani, M., & Ferrari, A. 2013, *MNRAS*, 436, 1102
- Mignone, A., Zanni, C., Tzeferacos, P., van Straalen, B., Colella, P., & Bodo, G. 2012, *ApJS*, 198, 7
- Ostriker, E. C., Stone, J. M., & Gammie, C. F. 2001, *ApJ*, 546, 980
- Porth, O. 2013, *MNRAS*, 429, 2482
- Pudritz, R. E. & Norman, C. A. 1983, *ApJ*, 274, 677
- Pudritz, R. E., Ouyed, R., Fendt, C., & Brandenburg, A. 2007, *Protostars and Planets V*, 277
- Quillen, A. C., Thorndike, S. L., Cunningham, A., Frank, A., Gutermuth, R. A., Blackman, E. G., Pipher, J. L., & Ridge, N. 2005, *ApJ*, 632, 941
- Rembiasz, T., Obergaulinger, M., Cerdá-Durán, P., Müller, E., & Aloy, M. A. 2016, *MNRAS*, 456, 3782
- Schuller, F., Menten, K. M., Contreras, Y., Wyrowski, F., Schilke, P., Bronfman, L., Henning, T., Walmsley, C. M., Beuther, H., Bontemps, S., Cesaroni, R., Deharveng, L., Garay, G., Herpin, F., Lefloch, B., Linz, H., Mardones, D., Minier, V., Molinari, S., Motte, F., Nyman, L.-Å., Reveret, V., Risacher, C., Russeil, D., Schneider, N., Testi, L., Troost, T., Vasyunina, T., Wienen, M., Zavagno, A., Kovacs, A., Kreysa, E., Siringo, G., & Weiß, A. 2009, *A&A*, 504, 415
- Sheikhnezami, S. & Fendt, C. 2015, *ApJ*, 814, 113
- 2018, *ApJ*, 861, 11
- Sheikhnezami, S., Fendt, C., Porth, O., Vaidya, B., & Ghanbari, J. 2012, *ApJ*, 757, 65
- Stepanovs, D. & Fendt, C. 2016, *ApJ*, 825, 14
- Stepanovs, D., Fendt, C., & Sheikhnezami, S. 2014, *ApJ*, 796, 29
- Tahani, M., Plume, R., Brown, J. C., & Kainulainen, J. 2018, *A&A*, 614, A100
- Wang, P., Li, Z.-Y., Abel, T., & Nakamura, F. 2010, *ApJ*, 709, 27
- Xu, J., Hardee, P. E., & Stone, J. M. 2000, *ApJ*, 543, 161
- Zanni, C., Ferrari, A., Rosner, R., Bodo, G., & Massaglia, S. 2007, *A&A*, 469, 811

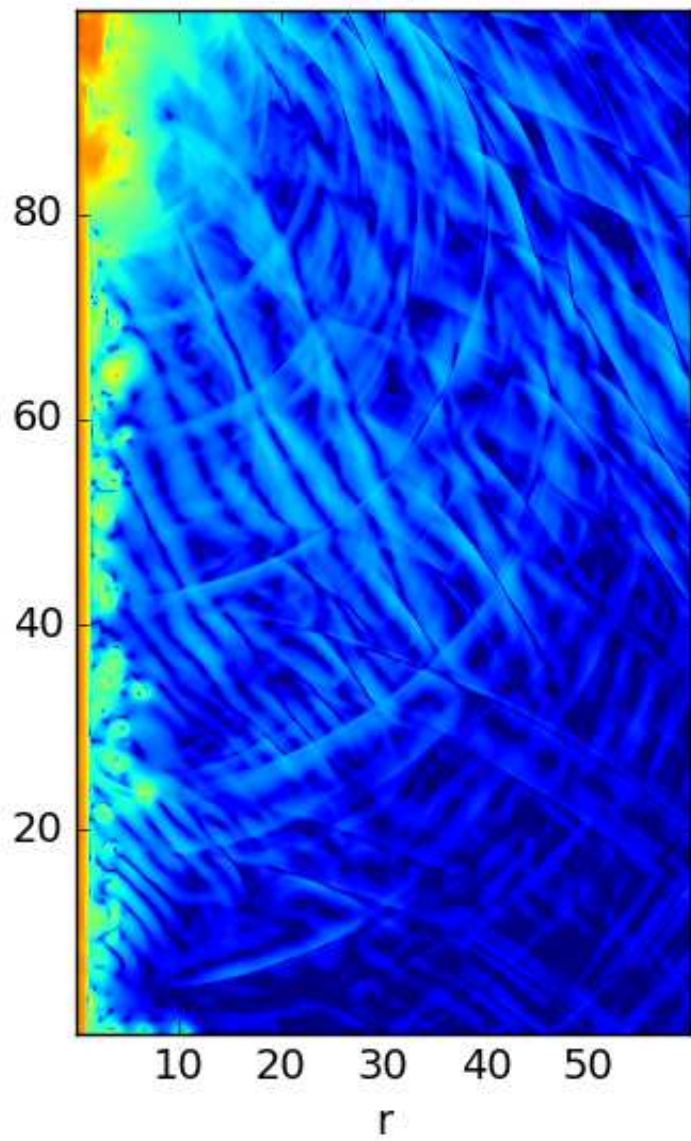
t=50



t=250



HD1



HD3

